ACS SyntheticBiology

pubs.acs.org/synthbio Research Article

ACtivE: Assembly and CRISPR-Targeted *in Vivo* Editing for Yeast Genome Engineering Using Minimum Reagents and Time

Koray Malcı, Nestor Jonguitud-Borrego, Hugo van der Straten Waillet, Urtė Puodžiūnaitė, Emily J. Johnston, Susan J. Rosser, and Leonardo Rios-Solis*

Cite This: *ACS Synth. Biol.* 2022, 11, 3629–3643 Read Online

ACCESS | Metrics & More | Article Recommendations | Supporting Information

ABSTRACT: Thanks to its sophistication, the CRISPR/Cas system has been a widely used yeast genome editing method. However, CRISPR methods generally rely on preassembled DNAs and extra cloning steps to deliver gRNA, Cas protein, and donor DNA. These laborious steps might hinder its usefulness. Here, we propose an alternative method, Assembly and CRISPR-targeted *in vivo* Editing (ACtivE), that only relies on *in vivo* assembly of linear DNA fragments for plasmid and donor DNA construction. Thus, depending on the user's need, these parts can be easily selected and combined from a repository, serving as a toolkit for rapid genome editing without any expensive reagent. The toolkit contains verified linear DNA fragments, which are easy to store, share, and transport at room temperature, drastically reducing expensive shipping costs and assembly time. After optimizing this technique, eight loci proximal to autonomously replicating sequences (ARS) in the yeast genome were also characterized in terms of integration and gene expression efficiencies and the impacts of the disruptions of these regions on cell fitness. The flexibility and multiplexing capacity of the ACtivE were shown by constructing a β-carotene pathway. In only a few days, >80% integration efficiency for single gene integration and >50% integration efficiency for triplex integration were achieved on *Saccharomyces cerevisiae* BY4741 from scratch without using *in vitro* DNA assembly methods, restriction enzymes, or extra cloning steps. This study presents a standardizable method to be readily employed to accelerate yeast genome engineering and provides well-defined genomic location alternatives for yeast synthetic biology and metabolic engineering purposes.

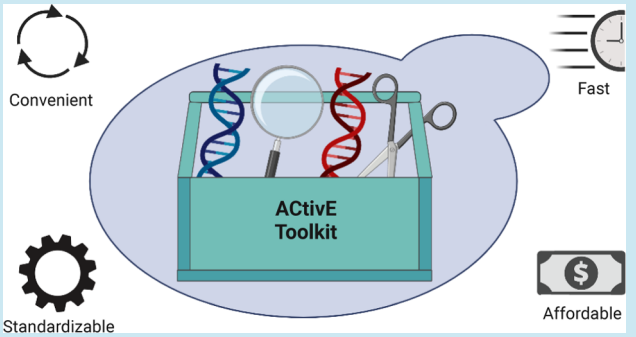

KEYWORDS: *Saccharomyces cerevisiae, CRISPR toolkit, genome editing, synthetic biology, standardization, locus characterization*

INTRODUCTION

Being a eukaryotic chassis, *Saccharomyces cerevisiae* has been extensively studied to produce high-value products from pharmaceuticals[1−4] to biofuels.[5−8] As a versatile and efficient genome engineering tool, the clustered regularly interspaced short palindromic repeats (CRISPR) system has been a widely used method to engineer yeast cell factories.[9,10]

In the past decade, a great number of CRISPR-based methods have been developed for yeast genome editing or cell factory development.[11,12] Mainly, delivery or expression of CRISPR-associated (Cas) protein, guide RNA (gRNA), and donor DNA differ in these yeast-specific CRISPR methods. Generally, Cas protein (generally Cas9), which is responsible for the nuclease activity on a specific genomic location,[13,14] is expressed through a plasmid vector[15,16] or genomic integration.[17,18] The latter needs an additional transformation for genomic integration and might lead to a burden on the host. gRNA forms a complex with Cas protein and guides it toward the target sequence,[13,14] and it is generally expressed by using plasmid vectors in the yeast. A single plasmid containing the genes of Cas protein and gRNA[16,19] or separate independent plasmids for each can be used with an additional selective marker.[20,21] Donor DNA is used as a DNA repair template for homology-directed repair (HDR)[22] after a double-strand break (DSB) is formed by Cas/gRNA complex. When it comes to delivery of donor DNA, single-strand oligos,[16] double-strand oligos,[23] or linear DNA fragments containing overlapping regions for *in vivo* assembly[24] can be used as well as linearized plasmids containing preassembled expression cassettes.[25]

Even though high efficiencies in genome editing or pathway construction were achieved with these methods, further research is needed, and more genetic parts should be characterized to reach a consensus.[11,12,26] On the other hand, the main obstacle in these methods is the requirement of *in vitro* DNA assembly and additional cloning steps to

Received: April 6, 2022
Published: October 17, 2022

https://doi.org/10.1021/acssynbio.2c00175
ACS Synth. Biol. 2022, 11, 3629−3643

construct CRISPR plasmids. Golden Gate assembly,[27] Gibson assembly,[28] or uracil-specific excision reaction-based cloning (USER cloning)[29] are the most widely used *in vitro* plasmid construction methods.[16,23,25,30−32] For instance, Ronda et al. (2015) developed the CrEdit method standing for CRISPR/Cas9 mediated genome editing, using the USER cloning to construct the CRISPR plasmids.[25] In another study, a Csy4-assisted CRISPR method was used for multiple genome editing, and the plasmid constructs were cloned using Gibson Assembly.[33] However, the use of these techniques needs additional steps, making the CRISPR process more labor-intensive and time-consuming. Moreover, these methods require relatively expensive DNA assembly kits[34,35] or specific type IIS restriction enzymes that might hinder design flexibility as the DNA fragment to be cloned might contain the recognition sites. Therefore, a collection of ready-to-use DNA parts skipping these preassembly steps can accelerate the genome editing process. Once this collection is obtained, it can also minimize the PCR deviations caused by the use of different DNA polymerases, which can be an important problem even though there are limited reports on this issue.[36] Finally, this toolkit based on verified DNA parts is more stable and practical to transport at room temperature for a prolonged period than glycerol stocks or agar slants. It can drastically reduce shipping costs while improving access to lower-income communities to contribute to synthetic biology's democratization.

In addition to how CRISPR is carried out, its genome editing efficiency is another critical issue. The sequence features of CRISPR RNA (crRNA), which has a base complementarity to the target DNA,[37] play a primary role in on-target efficiency and off-target specificity.[38] It has also been shown that gRNA expression might affect the CRISPR efficiency.[39] Apart from gRNA-dependent factors, target genomic loci might have an impact because of the chromatin structures.[40] Apel et al. (2017) found substantial variability in terms of integration efficiency and expression rate for 23 characterized genomic loci using green fluorescence protein (GFP) in *S. cerevisiae*.[41] Also, Wu et al. (2017) screened 1044 loci in the yeast genome, reporting important variations in RFP expression among the different loci tested.[42] Therefore, characterization of genomic regions in terms of CRISPR and gene expression efficiencies is crucial for identifying optimal target regions in the yeast genome. Especially for metabolic pathway construction involving many heterologous genes or extra copies of native genes,[2] the use of efficient loci is quite significant to improve production yield.

To accelerate the yeast strain development process, more convenient CRISPR methods reducing time, labor, and cost are necessary, as well as identification and characterization of optimal genomic loci for chromosomal integration of constructs. In the present study, we developed a modular, convenient, and standardizable CRISPR method, named Assembly and CRISPR-targeted *in vivo* Editing (ACtivE), relying on *in vivo* assembly of cotransformed DNA modules in yeast. We used chemically synthesized gRNA cassettes and synthetic overlapping fragments as connectors for *in vivo* DNA assembly. In this way, the modules can be easily selected and combined from a part repository depending on the application. Particular parts such as a module expressing a specific type of Cas protein or a gRNA module targeting a specific genomic region can be combined along with other modules to *in vivo* construct the CRISPR plasmid.

As the part repository contains only PCR-verified linear fragments, the use of plasmid purification kits to obtain the parts or extra enzymatic treatment steps such as DpnI digestion to degrade the parental plasmid is not necessary. Without the use of an agar stab/plate, this approach can also facilitate shipping. Also, compatible and custom-made parts can be exchanged between different groups thanks to the connectors (synthetic fragments) at the terminals of each module. This collection can serve as a CRISPR toolkit that will be expanded with new modules and is freely available at https://www.leorioslab.org/cost-crispr-toolkit/ so that users will be able to perform yeast genome editing by simply providing their own custom donor DNA. Therefore, ACtivE allows rapid and plasmid-free genome engineering in the yeast genome as it abolishes *in vitro* DNA assembly and cloning steps so that it does not require the use of type II restriction enzymes or DNA assembly kits, which can be a considerable expense for lower-income laboratory settings.

After optimizing the genome editing efficiency and reproducibility of the method, eight different genomic regions were characterized using a GFP, mNeonGreen, in terms of determining integration and gene expression efficiencies as well as integration effects on cell fitness. ∼80% single gene integration and deletion efficiencies were achieved. Furthermore, the multiplexing capacity of ACtivE was tested for simultaneous integration of multigenes into multiloci in the genome. The CRISPR technique used in this study enables standardizable and rapid genome engineering in the yeast genome, and thoroughly characterized genomic regions provide more alternatives to be used for genomic integration or pathway construction.

RESULTS AND DISCUSSION

Standardizable, Rapid, Convenient Yeast CRISPR. To create a CRISPR plasmid expressing the gRNA and Cas protein, *in vitro* DNA assembly procedures typically followed by a cloning step into *Escherichia coli* are the standard methods used in the yeast genome engineering processes. However, these steps retard this process, especially if sequential genome editing studies are needed to construct or design synthetic metabolic pathways. Here, we developed a more convenient, modular, and rapid CRISPR method, named Assembly and CRISPR-targeted *in vivo* Editing (ACtivE), which relies only on amplifying the functional units (DNA parts) through PCR. The modules contain small overlapping sequences assembled via *in vivo* HDR, so time-consuming and labor-demanding extra steps are omitted.

Gibson et al. (2008) succeeded in assembling a long, ∼600 kb, synthetic genome consisting of 25 overlapping fragments in yeast through HDR.[43] After this, Kuijpers et al. (2013) reported that using synthetic overlapping sequences increases the efficiency of *in vivo* DNA assembly in yeast.[44] In our design, we used five modules, a *Cas9* expression cassette, a gRNA expression cassette, a selection marker, a storage part, and a yeast origin of replication (ORI), to create an all-in-one CRISPR plasmid. 60 bp synthetic fragments[44] were used as overlapping sequences (connectors) between each adjacent module. Among them, selection marker and ORI are essential parts for surviving and propagating the plasmid, while Cas protein and gRNA are responsible for CRISPR activity. The storage part contains a bacteria-specific selection marker and ORI to be used for storage of the assembled plasmid in *E. coli* if desired. As chemical DNA synthesis is a rapidly growing

https://doi.org/10.1021/acssynbio.2c00175
ACS Synth. Biol. 2022, 11, 3629−3643

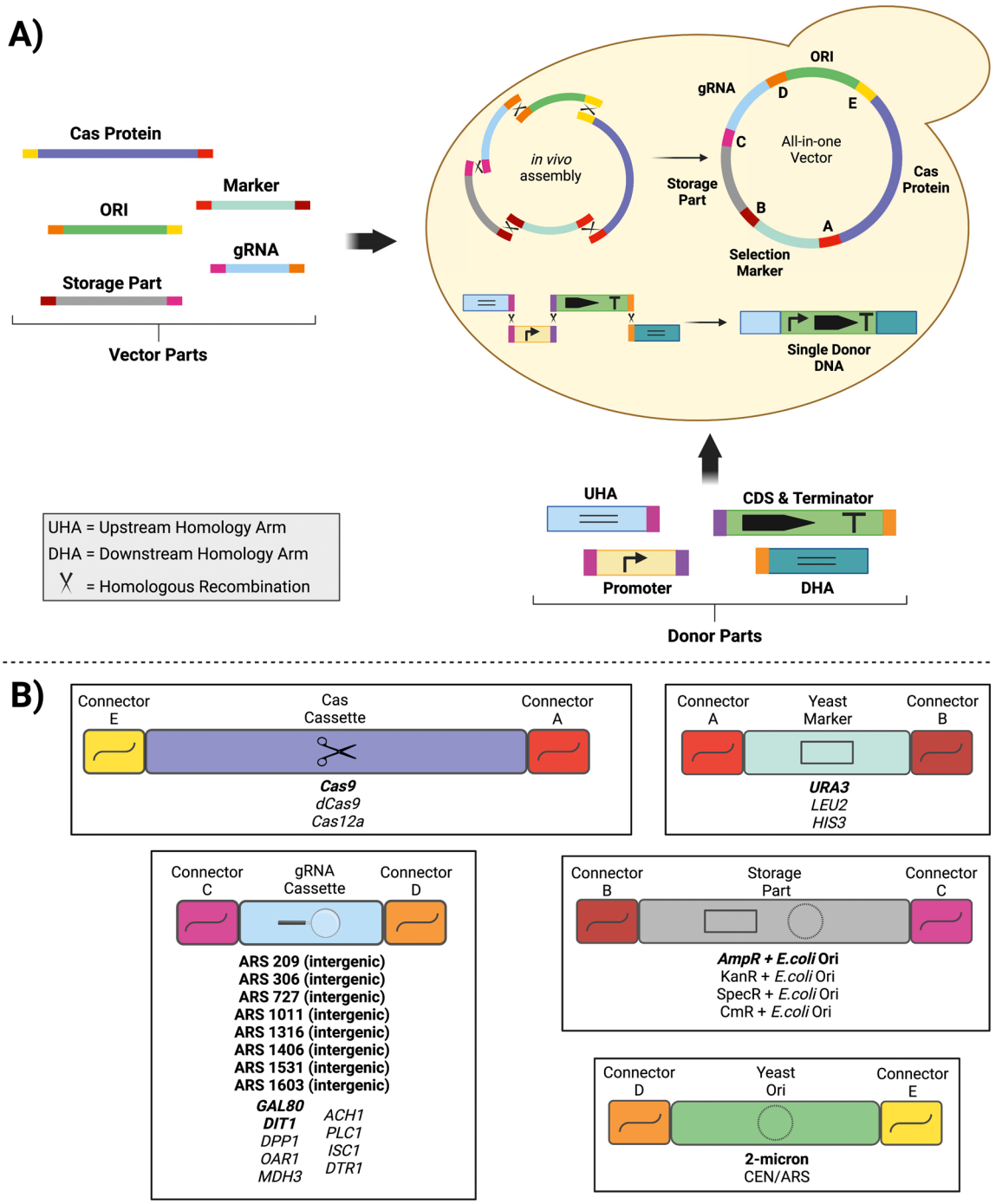

Figure 1. Overview of the ACtivE method. (A) Each plasmid module is produced by PCR and can be stored to create a part collection. The modules contain an overlapping sequence (connector) with their neighbor fragment for *in vivo* assembly via homologous recombination. Depending on the application, the plasmid modules can be selected from the part collection. In this study, the donor DNA consisted of four parts, and they were cotransformed with plasmid modules in a single transformation step. In yeast, the parts are assembled via homologous recombination, and the donor DNA is inserted into the genome thanks to its homology arms with the genome. The length of the parts may not represent the actual sizes. (B) The parts provided in the first version of the ACtivE toolkit (the parts in bold were characterized in this study). The gRNAs of ARS-proximal regions target intergenic regions in the genome, whereas other gRNAs target the genes. The gRNAs are driven by *SNR52p*. By providing their own custom repair donor DNA, the users can readily combine the plasmid modules depending on their applications for a rapid yeast genome editing study. The toolkit will be expanded with new parts and is freely available with more information at https://www.leorioslab.org/cost-crispr-toolkit/.

sector[45] with many alternative approaches,[46] synthetic production of expression cassettes can be a reasonable and affordable choice, especially for short fragments, 300−500 bp, compared to traditional constructing methods. Therefore, synthetic gRNA expression cassettes were used in our method, allowing the users to choose any integration locus they desire in addition to the eight ones characterized in this work. When it comes to donor DNA to integrate heterologous genes of interest (GoI), we used four parts, ∼1000 bp upstream homology arm (UHA), promoter, CDS + terminator, and

https://doi.org/10.1021/acssynbio.2c00175
ACS Synth. Biol. 2022, 11, 3629−3643

Table 1. crRNA Sequences Used in This Study to Integrate *mNeonGreen* and Sequence Features[a,b]

Target Region	Sequence 5' – 3'	Chromosome	MIT Specificity Score[52]	Efficiency Prediction Scores		Off-target mismatches
				Doench[51]	Moreno-Mateos[50]	
ARS 209	ATAAAATGTGCTAGAACGTA *TGG*	II	100	51	54	0
ARS 306	GTTAGGAGAAGGAGCGGGTC *TGG*	III	100	44	66	0
ARS 727	CCGCGCCACTGCTATGACAA *CGG*	VII	100	61	67	0
ARS 1011	CTGGCGCTGCTGGAAGTGAA *TGG*	X	100	56	69	0
ARS 1316	ATAGTTACTACCTAAGAAGT *GGG*	XIII	100	65	56	0
ARS 1406	ACGGTTCTGATGGGAATGCA *GGG*	XIV	100	52	67	0
ARS 1531	GGCCTCGGCAACTTTCAGGG *GGG*	XV	100	64	63	0
ARS 1603	GCAAGAACGAAGCTAACGAG *AGG*	XVI	100	70	58	0

[a]The last three nucleotides in red represent the PAM sequences. [b]The scores are out of 100.

~1000 bp downstream homology arm (DHA). In this way, individual promoter parts could be easily changed as a widely used approach for fine-tuning gene expression.[47] Similar to plasmid assembly, each donor part had a 60 bp overlapping sequence (Table S3 and S4) with its adjacent part to abolish the use of *in vitro* assembly methods. The overlapping fragments between the donor DNA parts should be sequence-specific for a scar-free assembly depending on the donor DNA, as we could not detect protein expression when 60 bp synthetic sequences were used for donor DNA assembly (data not shown). Therefore, the ACtivE toolkit contains CRISPR plasmid modules; users should provide their own custom donor DNAs. Figure 1 illustrates the working principles and design of ACtivE and the content of the toolkit provided. Once plasmid modules are produced, they can be stored for subsequent study. Indeed, one of the benefits of this design is that the CRISPR plasmid construction can be readily standardized by using the connectors (synthetic fragments) and a part collection containing different alternatives for each module. For instance, the Cas cassette has connector A and connector E at the terminals. Depending on the purpose, a particular type of Cas protein, Cas9, dead Cas9, Cas12a, etc., could be selected from the collection to be combined with other modules. This also applies to other parts, such as the selection markers, allowing more flexibility and part exchange between different research groups. Moreover, as the method relies on only *in vivo* assembly and PCR for the donor DNA, the whole process can be finished in a single day with a good organization from scratch. Nevertheless, it should be noted that *in vitro* DNA assembly methods can still be used for the donor DNAs, as the overlapping fragments between the donor DNA parts are sequence-specific.

Selecting Integration Regions. To integrate the GoI, *mNeonGreen*, into the yeast genome, eight loci on eight different chromosomes were selected to compare the integration and gene expression efficiency and impact on cell fitness. Previous studies reported that gene expression rates of heterologous genes tend to be higher if they are located in a region close to autonomously replicating sequences (ARS).[48,49] Therefore, eight ARS-proximal intergenic regions that were not characterized before were randomly selected and were targeted for integrations. crRNA sequences (20 bp) on these regions were scored using different algorithms. Moreno-Mateos et al. (2015) developed a gRNA activity prediction algorithm, CRISPRscan, using zebrafish-specific gRNAs, giving higher efficiency scores if the crRNA sequence has high guanine but low adenine content,[50] whereas Doench et al. (2016) used mammalian cells to develop a gRNA efficiency algorithm.[51] Both algorithms were considered for selecting crRNAs as yeast-specific algorithms have not been developed yet. To minimize the off-target effects in the genome, the sequences that have the maximum MIT scores representing the highest uniqueness were selected.[52]

Table 1 shows the crRNA sequences used in this study and their corresponding scores. The sequences were selected considering the highest specificity and efficiency prediction scores among the other crRNA sequences on the regions.

Optimization of the Method. The integration efficiency of ACtivE was first tested on three loci, ARS306, ARS1316, and ARS1603, using high-fidelity Phusion polymerase to amplify plasmid modules and the donor DNA parts (Figure 1). Even though the GoI was successfully integrated into all regions, the integrations efficiencies ranged from 35% to 41% (Figure 2A). Stratigopoulos et al. (2018) reported that 24 h of DMSO feeding prior to CRISPR increased mammalian cell genome editing efficiency.[53] We, therefore, first tested whether DMSO feeding for 24 h had a positive effect on CRISPR efficiency for *S. cerevisiae*. Unfortunately, DMSO feeding resulted in lower integration rates with less than 30% (Figure 2A). Also, ~50% fewer colonies were obtained after transformation compared to the DMSO-free method. Following that, the false positive colonies, which were able to grow on the selective media but did not express *mNeonGreen*, were further studied to determine whether they contained correctly assembled Cas9 plasmid, using primers flanking the overlapping sequences, connectors, as indicated in Figure 2B. This revealed that none of the false-positive colonies contained connector A, and only ~10% of them had connector E in their plasmids. As both connectors were overlapping sequences flanking the *Cas9* cassette, we then tested if the *in vitro* plasmid parts could be amplified in full. The plasmid parts were used as a template, and ~20 bp primers at the end of the terminals were used for a second PCR, as demonstrated in Figure 2C. Although the four plasmid parts, selection marker, yeast ORI, storage part, gRNA, were amplified, the Cas9 gene failed. In contrast, it was amplified from a correctly assembled plasmid, proving that the terminal sequences of the Cas9 gene (connector A and E) were not completely amplified by the Phusion polymerase. Indeed, there are limited studies about inefficient, repetitive PCR problems, which have contributed to the lack of reproducibility in certain assays in the synthetic biology community.[54,55] Shevchuk et al. (2004) reported the

https://doi.org/10.1021/acssynbio.2c00175
ACS Synth. Biol. 2022, 11, 3629−3643

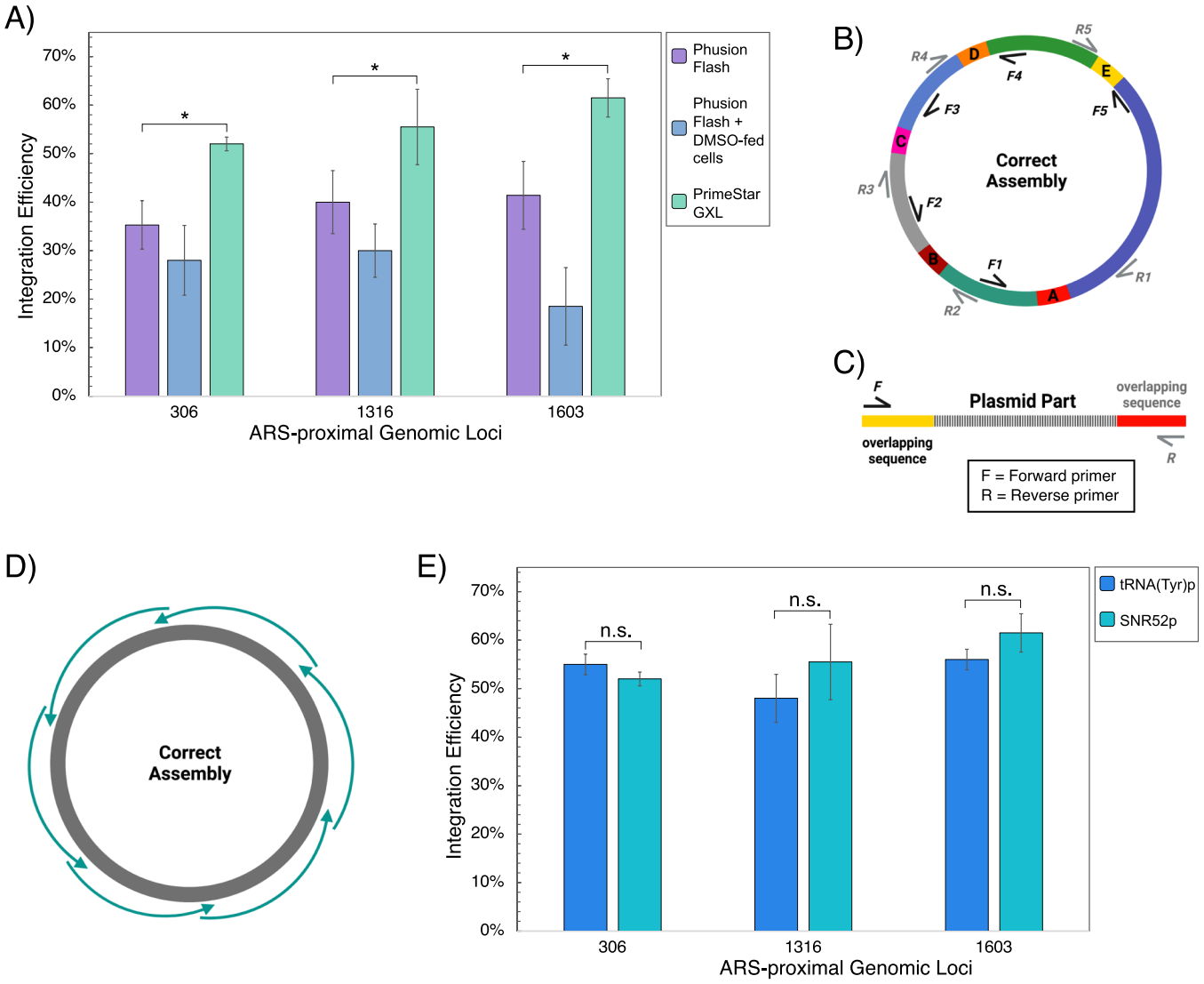

Figure 2. Optimization process and results of ACtivE. (A) Comparison of integration efficiencies of different conditions; Phusion polymerase-based plasmid parts, DMSO feeding for 24 h for Phusion polymerase-based plasmid parts, and PrimeSTAR GXL-based plasmid parts. (B) The all-in-one CRISPR plasmids were screened using plasmid colony PCR primers (F1−5, R1−5) targeting the connectors between adjacent plasmid modules. (C) Each plasmid part was controlled to determine whether they were amplified in full after PCR reactions using ∼20 bp primers annealing at the end of the synthetic overlapping sequences. (D) Whole plasmid sequencing with primer walking using Sanger sequencing to confirm the correct assembly and the sequence of the assembled construct. (E) Comparison of integration efficiencies when gRNA is expressed by two different promoters, *SNR52p* or $tRNA^{(Tyr)}p$. The values are displayed as the mean of triplicate experiments, and error bars represent standard deviations. For simplification, ARS regions are shown with their corresponding numbers. The single asterisk represents a *p*-value <0.01 and "n.s." stands for not statistically significant (*p*-value >0.05). The error bars show the standard deviations of three replicates.

"shortening phenomenon" for PCR products.[36] Researchers revealed that the amplicons of high-fidelity DNA polymerases might yield truncated products because of the shortening of the amplicon's ends, especially for relatively long targets (>3−4 kb).[36] For this reason, we applied two alternative approaches (i) using longer primers (∼120 bp ultramers, Table S1) containing nonfunctional extra bases at the terminal to nullify the shortening, (ii) dividing the long Cas9 gene with internal primers (Table S1) into two parts resulting ∼2.5 kb fragments. However, none of these strategies resulted in higher integration rates since integration rates similar to those of Phusion polymerase are achieved. Finally, we tested another high-fidelity DNA polymerase, PrimeSTAR GXL, which has a relatively higher error rate compared to Phusion. Surprisingly, it successfully amplified the Cas9 gene in full (Figure 2A), and all plasmid parts were reamplified with a second PCR, as explained above. Consistently, the integration efficiencies in all regions increased by approximately 1.5 fold (*p*-value <0.01), as shown in Figure 2C. Thus, all the plasmid parts were produced using PrimeSTAR GXL in the subsequent experiments, while donor DNA parts were produced using Phusion polymerase.

Following improving the integration efficiency, false-positive colonies were screened to see if they contained the correctly assembled CRISPR plasmid after using the PrimeSTAR GXL. It was observed that ∼95% (18 out of 19 colonies) of the false-positive colonies had incorrectly assembled plasmids without gRNA and/or Cas9 parts, and all positive mNeonGreen expressing colonies contained correctly assembled plasmids (10 out of 10 colonies). According to the manufacturers, the error rate of the Phusion Flash DNA polymerase is $\sim 1 \times 10^{-6}$,

https://doi.org/10.1021/acssynbio.2c00175
ACS Synth. Biol. 2022, 11, 3629−3643

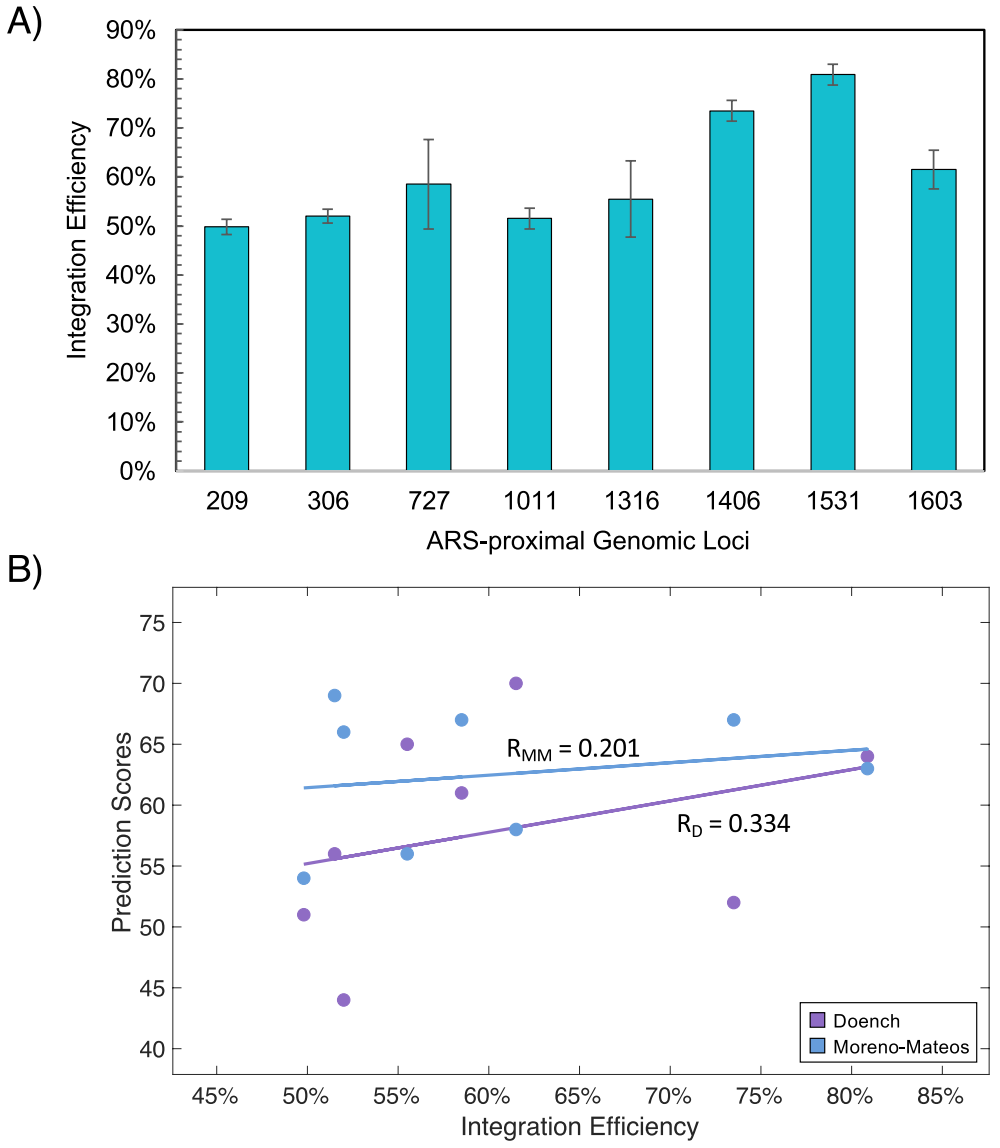

Figure 3. Integration efficiencies and their correlation with prediction algorithms. (A) Integration efficiency of *mNeonGreen* on eight ARS-proximal genomic loci. The values are displayed as the mean of triplicate experiments and error bars represent standard deviations. For simplification, ARS regions are shown with their corresponding numbers. (B) Linear regression models showing the correlation between integration percentages and gRNA efficiency scores of Doench's[51] and Moreno-Mateos'[50] prediction algorithms. R_D = Pearson correlation coefficient based on Doench's algorithm, R_{MM} = Pearson correlation coefficient based on Moreno-Mateos' algorithm. The error bars show the standard deviations of three replicates.

and it is ~6×10^{-5} for the PrimeSTAR GXL. Therefore, whole plasmids from one positive (mNeonGreen expressing) colony and one negative (false-positive) colony were sequenced by Sanger sequencing using primer walking (Figure 2D) to further investigate the error rates and confirm the correct assembly. This verified that the plasmid in the positive colony was correctly assembled, and there was no priming on the Cas9 module on the plasmid from the negative colony. Neither plasmid contained PCR-caused error; also, the mutations that can occur might be silent or on a sequence that does not have a critical function on the plasmid. Therefore, this also showed that the accuracy of *in vivo* plasmid assembly was the critical factor for CRISPR success in our method.

On the other hand, the false-positive colonies indicated that the plasmid could be assembled with missing parts. Different combinations of plasmid parts were transformed into yeast cells to confirm this. Although transformation yield dramatically decreased with missing parts, we observed a small number of colonies as long as they contained a selection marker and yeast ORI that are essential parts for surviving, as demonstrated in Figure S5. This was probably because of assembling the plasmid parts through nonhomologous end-joining (NHEJ) rather than HDR.[56,57] NHEJ is a well-studied pathway, and the genes involved in this process are elucidated.[56,57] Therefore, as a further improvement, a disruption in the NHEJ pathway could increase the integration efficiency of ACtivE or similar methods, as shown previously for a nonconventional yeast *Yarrowia lipolytica*.[58]

Additionally, we also compared two RNA expressing promoters to determine whether they affected gRNA expression and CRISPR activity as the differences in the promoters' features might have an impact on the expression.[38] SNR52 RNA polymerase III promoter (*SNR52p*) is one of the most widely used promoters to express gRNAs in yeast.[12,23]

https://doi.org/10.1021/acssynbio.2c00175
ACS Synth. Biol. 2022, 11, 3629−3643

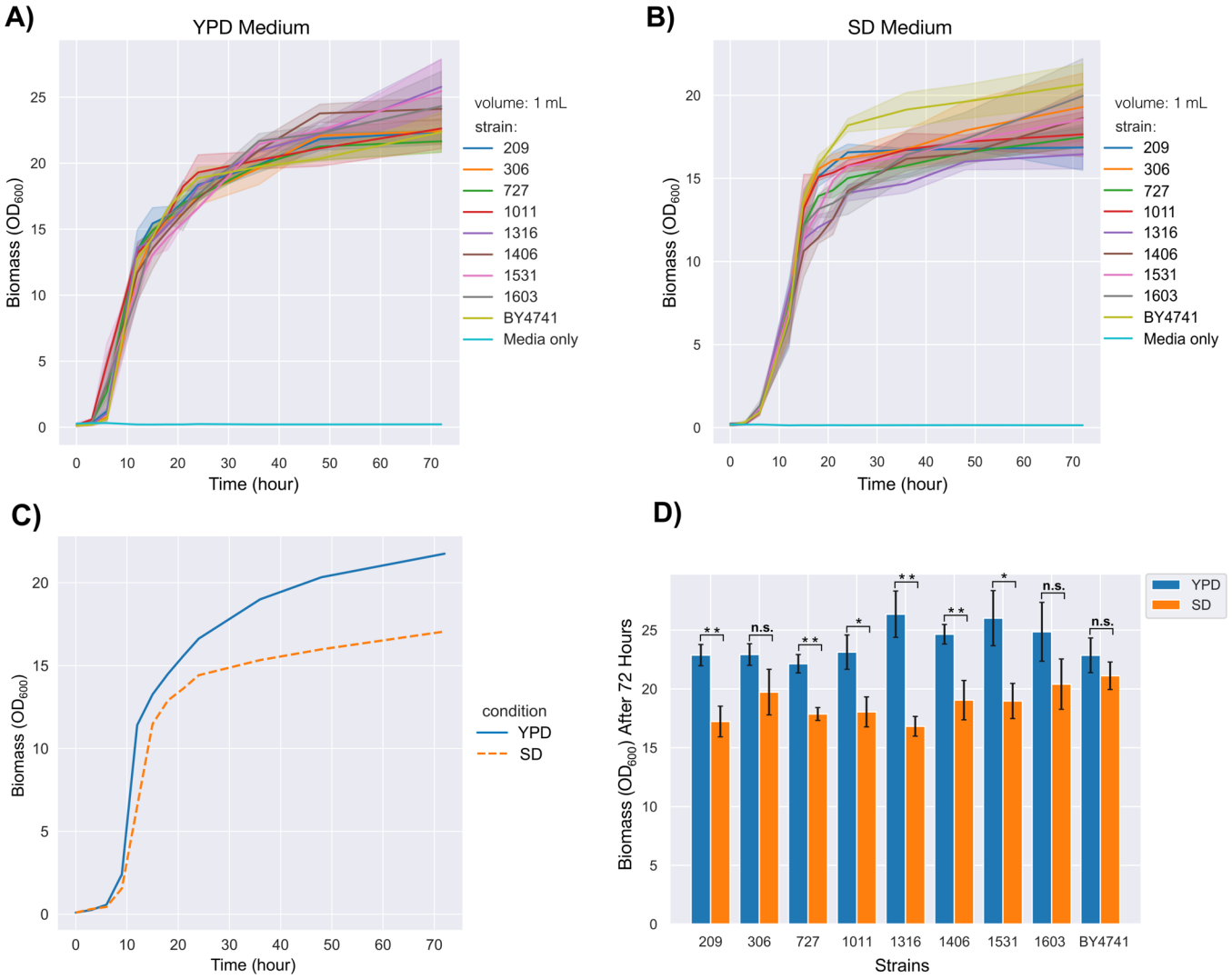

Figure 4. Biomass comparison between *mNeonGreen* integrated strains and the parental strain. (A) The biomass over 72 h in YPD media. (B) The biomass over 72 h in SD media. (C) Growth trends in YPD and SD media comparing mean biomass of all strains in these two conditions over 72 h. (D) The final OD_{600} values represent the total biomass after 72 h. The experiments were conducted in 1 mL wells in microplates. The single asterisk represents a *p*-value <0.05, double asterisks represent a *p*-value <0.01, and "n.s." stands for not statistically significant (*p*-value >0.05). The standard deviations of the three replicates are shown by shading on the curves or by error bars on the bar chart. The solid lines on the curves stand for the average values of independent colonies or different strains.

Alternatively, gRNAs can be transcribed using tRNA promoters.[11,41] Therefore, we tested *SNR52p* and $tRNA^{(Try)}$ promoters as shown in Figure 2D; however, no statistically significant difference (*p*-value >0.05) was observed. Therefore, *SNR52p* was used for further experiments and in the toolkit. Dong et al. (2020) compared $tRNA^{(Try)}$, $tRNA^{(Pro)}$, and *SNR52* promoters in terms of disruption yield on the *ADE2* gene and repression efficiency on a heterologous fluorescence protein.[59] Consistent with this study, researchers found very similar disruption and repression yields with these three gRNA promoters.[59] *SNR52p* consists of 269 bp, while $tRNA^{(Try)}p$ contains 118 bp (Figure S1). Therefore, promoters such as $tRNA^{(Try)}p$ could be used to minimize the cost of the synthetic gRNA cassettes.

Integration Efficiencies on Eight ARS-Proximal Genomic Loci. The optimized ACtivE method as mentioned above was used to integrate *mNeonGreen* into five more ARS-proximal genomic loci to compare the integration efficiencies and characterize the selected eight genomic regions (Table 1). High-yield gene integrations ranging from 50% to 80% were achieved in the target regions, as shown in Figure 3A. Although 100% gene integration or deletion efficiencies have been previously reported,[12] genome editing efficiency of ACtivE is remarkably high considering its convenience and rapidity. In addition, previous works reported extremely low (<20%) CRISPR-based heterologous gene integration efficiencies in some genomic locations.[41] Therefore, the regions tested in this study are suitable targets for gene integrations.

The relationship between integration efficiencies and gRNA efficiency scores of the genomic regions (Table 1) was also determined using linear regression models, as shown in Figure 3B. Moderate and weak positive correlations were found on Doench[51] and Moreno-Mateos[50] algorithms with a Pearson's correlation coefficient of $R = 0.334$ and $R = 0.201$, respectively. These findings evaluating a small data set can be considered promising, although the best fitting gave only a moderate positive correlation. These findings suggest that computational gRNA design/scoring tools can help with selecting gRNA

https://doi.org/10.1021/acssynbio.2c00175
ACS Synth. Biol. 2022, 11, 3629−3643

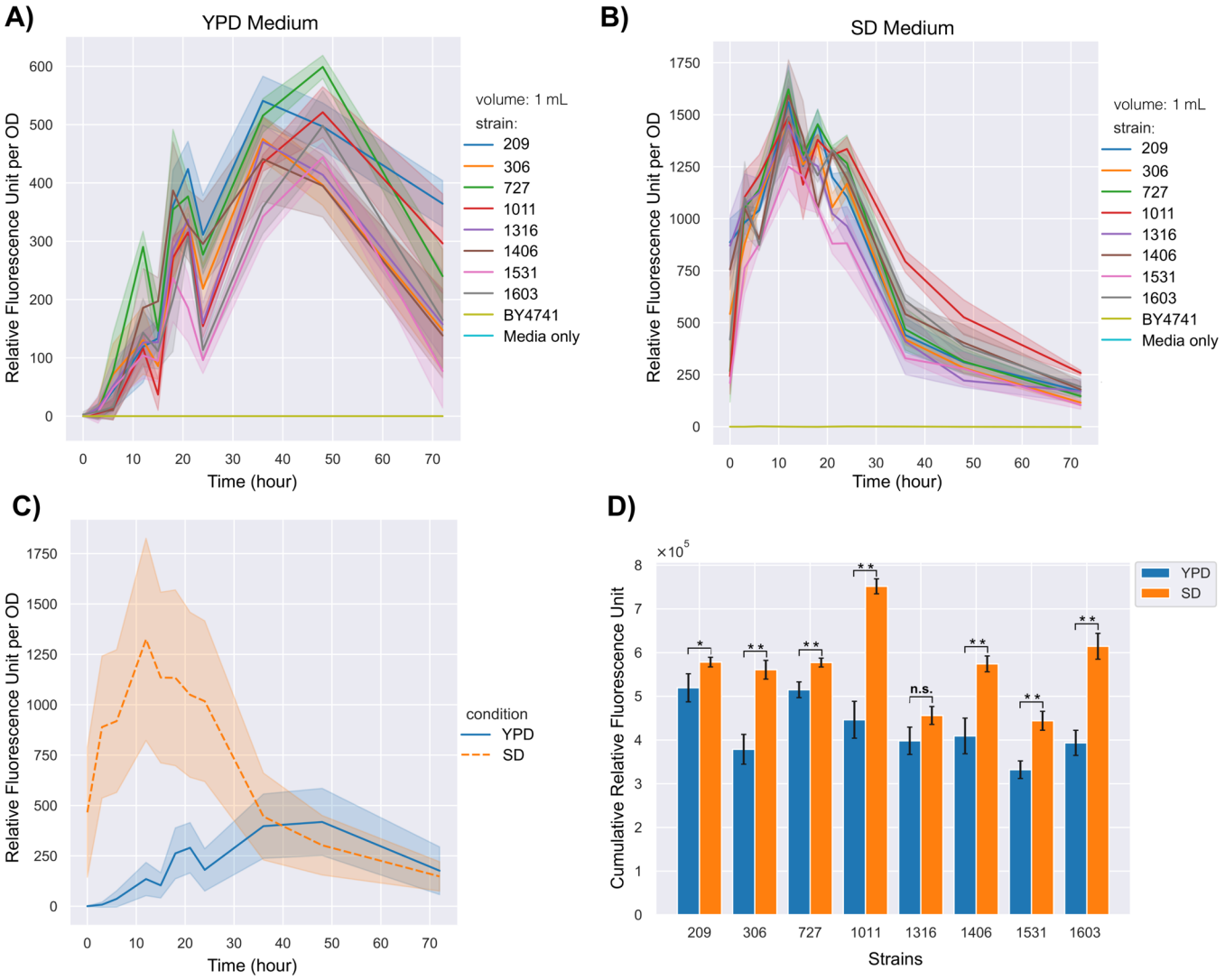

Figure 5. Comparison of heterologous gene expression between *mNeonGreen* integrated strains. (A) Relative fluorescence intensities (RFU) over 72 h in YPD media. (B) RFUs over 72 h in SD media. (C) The average RFUs of all strains in YPD and SD media separately. (D) The cumulative RFU values represent the total gene expression or protein production by the total biomass at each time for 72 h. The experiments were conducted in 1 mL wells in microplates. The single asterisk represents a *p*-value <0.05, double asterisks represent a *p*-value <0.01, and "n.s." stands for not statistically significant (*p*-value >0.05). The standard deviations of the three replicates are shown by shading on the curves or by error bars on the bar chart. The solid lines on the curves stand for the average values of independent colonies or different strains.

sequences for CRISPR-based studies in yeast, considering the algorithms' limitations. Nevertheless, a larger sample size is required to evaluate these prediction algorithms properly. 3-D chromatin structures of the yeast[60] might also be taken into consideration to develop more reliable yeast-specific prediction tools.

Characterization of Genomic Loci. The genomic regions used as landing pads for *mNeonGreen* were characterized in terms of gene expression rate and effect on the cell fitness in two different media, YPD and SD, as described in the Materials and Methods section. First, plasmid-free cells were selected using 5-FOA counter-selection to eliminate plasmid burden. OD_{600} was measured to compare biomass and growth rates of the strains containing *mNeonGreen* on different genomic loci. Figure 4 shows the biomass of the yeast strains in YPD and SD media.

As seen, the growth curves presented the expected trends in both media (Figure 4A and 4B). The average biomass (Figure 4C) of nine strains, including the parental strain, BY4741, was expectedly higher in YPD media compared to SD media (*p*-value <0.01) as YPD is a richer environment than SD media.[61,62] The biomass order in YPD media was as follows:

$$1316 > 1531 > 1603 > 1406 > 1011 > \text{BY4741} > 306 > 209 > 727$$

Although the 1316 ($OD_{600} \approx 26$) showed the highest biomass, and the 727 ($OD_{600} \approx 22$) showed the lowest biomass at the 72nd hour (Figure 4A), there were no statistically significant differences when they were compared to the parental strain ($OD_{600} \approx 22.5$) (*p*-value >0.05). These data showed that perturbations on these genomic loci are unlikely to cause a negative effect on cell fitness considering the parental strain. Apel et al. (2017) reported a similar result as they did not find a significant difference in growth rates of GFP expressing strains compared to their parental strain in YPD media.[41] However, a statistically significant difference (*p*-value <0.05) was observed between the 1316 and the 727, showing

https://doi.org/10.1021/acssynbio.2c00175
ACS Synth. Biol. 2022, 11, 3629−3643

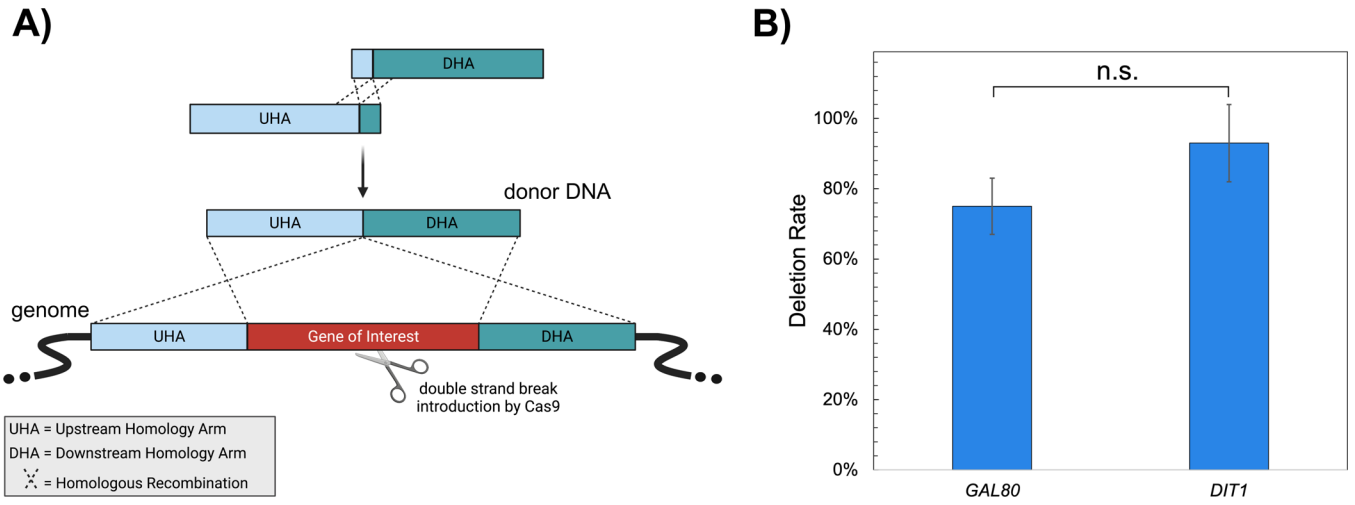

Figure 6. (A) The illustration of gene deletion using ACtivE. (B) Gene deletion rates on *GAL80* and *DIT1* genes. "n.s." stands for not statistically significant (p-value >0.05).

that targeting ARS1316 likely yields better biomass than ARS727 in YPD media.

On the other hand, the average biomass order in SD media was as follows:

$$\text{BY4741} > 1603 > 306 > 1406 > 1531 > 1011 > 727 > 209 > 1316$$

BY4741 showed the highest biomass amount as the parental strain in SD media (Figure 4B). A statistically significant difference (p-value <0.05) was observed when the parental strain BY4741 was individually compared with 209, 727, 1011, and 1316, meaning that genetic perturbations on these loci might negatively affect the cell fitness in SD media. Surprisingly, 1316 resulted in the lowest biomass in SD media even though it was the best growing strain in YPD. Also, a substantially different biomass order was observed in SD media compared to YPD media (Figure 4D). These results show that genetic alterations in the corresponding locations might distinctly affect the cell fitness of yeast strains depending on the environmental conditions and the media compositions.

In addition, the growth rates of the strains were calculated using a Gaussian process-based algorithm.[63] As shown in Figure S6, the maximum growth rate of BY4741 was observed around the sixth hour in both YPD and SD media. Similarly, the maximum growth rates of *mNeonGreen* integrated strains were at the sixth hour in SD media (Figure S8). However, 1011, 1406, 1531, and 1603 showed the maximum growth rate at around the third hour, whereas the others were around the sixth hour (Figure S7). Probably, perturbations on ARS1011, ARS1406, ARS1531, and ARS1603 affect the growth rate in YPD media.

To compare gene expression, fluorescence intensities produced by mNeonGreen were measured. Autofluorescence caused by the yeast cell itself and the media[64] was corrected using *omniplate*[65] to detect the fluorescence intensity per OD.

All strains showed similar expression patterns based on the selected medium, YPD or SD, with some fluctuations in the first 24 h, as shown in Figures 5A and 5B. As mNeonGreen expression was driven by the constitutive *TDH3* promoter in all mNeonGreen expressing strains, these results also showed the expression patterns of *TDH3p* in YPD and SD media (Figure 5C). In YPD media, the best mNeonGreen expressing strains depended on the hour. For instance, at 24th, 36th, and 72nd hours, the 209 was the best strain for mNeonGreen expression, whereas the 727 showed the highest expression at the 48th hour (Figure 5A). These two strains were also the most mNeonGreen producing strains in 72 h (Figure 5D).

The 1011 showed the highest expression from the 24th hour in SD media (Figure 5B). Therefore, the ARS1011 was the best integration site for the cumulative expression of mNeonGreen in SD media even though the 1011's biomass was significantly lower than the parental strain (p-value <0.05) in SD media (Figure 4D). Moreover, Figures 4C and 5C show that more biomass was obtained in YPD media. Still, mNeonGreen expression was dramatically higher in SD media as there was a significant difference in expression rates in the first 36 h of SD and YPD media. This shows that the expression rates were maximum in the exponential phase in SD media. Thus, SD media seems to be more advantageous for cumulative protein production than YPD media for these genomic loci.

Locus-based, *TDH3p*-driven heterologous gene expression in the yeast genome has been thoroughly studied in this work presenting biomass, fluorescence intensity per OD, expression rate, and cumulative expression in 72 h with 11 different time points in two different media. These findings can also give insights into the expression patterns of the native *TDH3* gene that encodes an enzyme, glyceraldehyde 3-phosphate dehydrogenase, involved in glycolysis, transcriptional silencing, and rDNA recombination.[66]

Single-Step Gene Deletion Using Only Homology Arms. In addition to genomic integration, gene deletion was also tested using ACtivE. To this end, two nonessential genes, the *GAL80* gene encoding a regulator protein for galactose-related metabolic genes[67] and the *DIT1* encoding a sporulation-specific enzyme,[68] were deleted. Using only UHA and DHA flanking outside the genes (primers and crRNAs are listed in Table S5), ∼75% deletion efficiency and ∼93% deletion efficiency were achieved for the *GAL80* and *DIT1* genes, respectively, without the need for any heterologous gene part. In this way, the whole *GAL80* and *DIT1* genes were deleted without any scar. The deletions were confirmed using colony PCR and Sanger sequencing. This study demonstrates

https://doi.org/10.1021/acssynbio.2c00175
ACS Synth. Biol. 2022, 11, 3629−3643

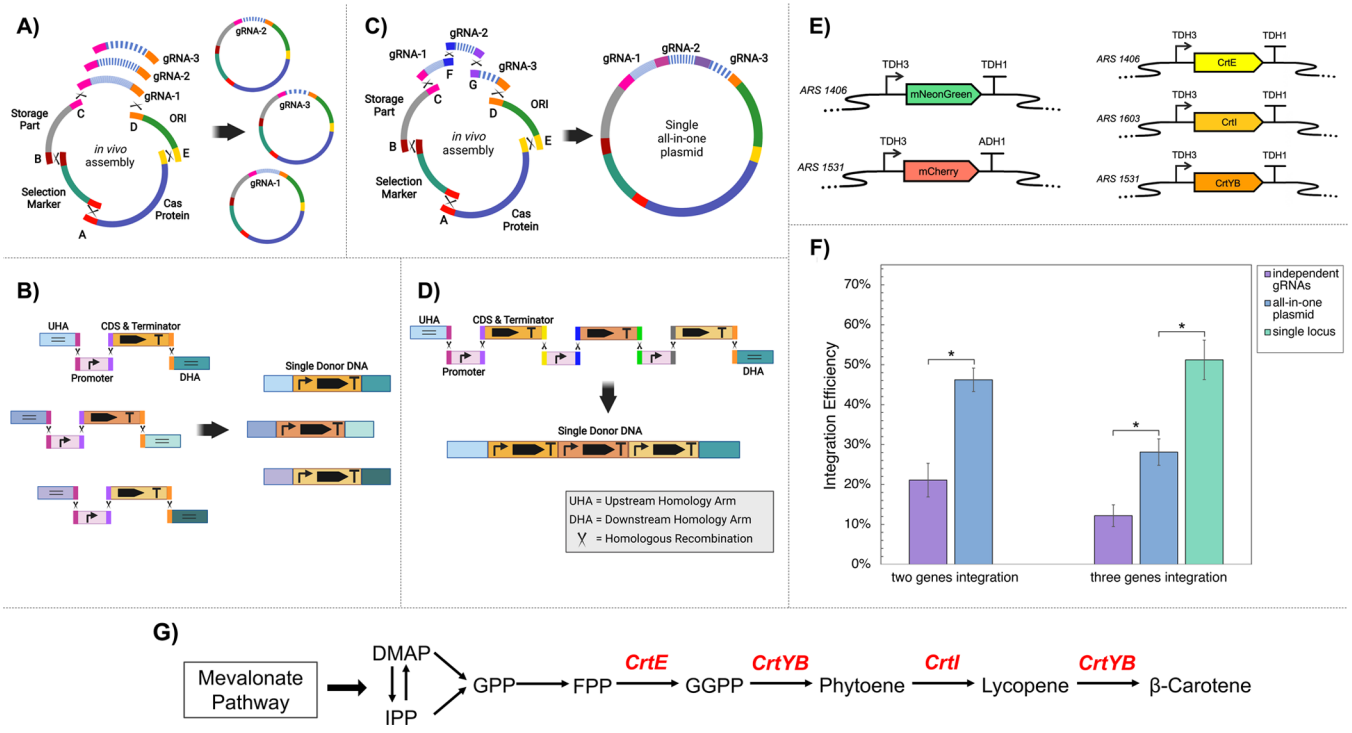

Figure 7. Multiplexing approaches and efficiencies. (A) Different gRNA cassettes are *in vivo* assembled, resulting in different plasmids targeting multiple loci. Each gRNA cassette contains identical overlapping sequences at their terminals so that each one individually assembles with the other plasmid parts. (B) For multilocus and multigene integration, each gene has its own homology arms (HA) depending on the target site. (C) The gRNA cassettes are tandemly assembled, resulting in a single all-in-one plasmid that targets multiple loci. (D) The promoters and CDSs can be tandemly assembled for single-locus multigene integration. The multigene cassette contains a single upstream homology arm (UHA) and downstream homology arm (DHA). (E) Genetic construct illustrations of *mNeonGreen* and *mCherry* genes used for single-step double gene integration and *CrtE*, *CrtI*, and *CrtYB* genes used for single-step triple gene integration. (F) Integration efficiencies achieved using different strategies. The single asterisk represents a *p*-value <0.01. The error bars show the standard deviations of three replicates. (G) The heterologous *β*-carotene pathway constructed in a single-step multigene integration. The heterologous genes are shown in red.

the flexibility of ACtivE as the same approach can be also used for scar-free gene deletion.

Multiplexing Using ACtivE. Simultaneous genome alterations in a single step can be preferential to accelerate genome editing or heterologous pathway construction. Therefore, the multiplexing capacity of ACtivE was tested for multiloci and multigene integrations into the yeast genome using different plasmid assembly and donor DNA delivery strategies, as illustrated in Figure 6. Initially, two fluorescent reporter proteins, mNeonGreen and mCherry, were integrated into ARS1406 and ARS1531 loci, respectively (Figure 7E), using two independent gRNA modules to be assembled into two different plasmids (Figure 7A). With this strategy, *mNeonGreen* and *mCherry* were simultaneously integrated into 21% of the colonies (Figure 7F). Alternatively, the gRNAs targeting ARS1406 and ARS1531 were *in vivo* assembled using synthetic homology sequences resulting in a single all-in-one plasmid expressing both gRNAs simultaneously (Figure 7C). The integration rate reached 46% with this approach (Figure 7F).

Following this approach, three heterologous genes of the *β*-carotene pathway, *CrtE*, *CrtYB*, and *CrtI* (Figure 7G), were simultaneously integrated into ARS1406, ARS1531, and ARS1603, respectively. A 12% integration rate was achieved using the strategy of assembling independent plasmids for each gRNA (Figure 7A), but this increased to 28% when three gRNAs were assembled in a single plasmid (Figure 7C). Furthermore, the genes were integrated into a single locus (ARS1531) to construct the multigene pathway on a single genomic location (Figure 7D), and 51% of the colonies successfully produced the orange pigment. Indeed, the differences in integration efficiencies were not surprising as higher integration rates were observed with fewer linear fragments. Even though the 12% integration rate is relatively low, the correct assembly and/or integration of 19 linear fragments (Figure 7A and 7B) shows the flexibility and capability of the ACtivE method.

CONCLUSION

The ACtivE method proposes a practical strategy to accelerate yeast genome engineering. It eliminates the use of any reagents or kits used for *in vitro* DNA assembly and bypasses extra cloning steps. Therefore, verified linear fragments have been collected to create a flexible CRISPR toolkit for many different purposes. The first version of the toolkit and a user manual are freely available at https://www.leorioslab.org/cost-crispr-toolkit/. The user can simply combine the modules provided in the toolkit without any plasmid purification, enzymatic treatment, *in vitro* assembly, or cloning steps. Providing custom donor DNA, the whole work for genome editing can be completed in only 1 day using verified linear fragments. Moreover, the modules to be used for CRISPR plasmid construction can be stored for a long time for further applications, and they can be exchanged between different groups as standard parts thanks to their synthetic ends. In this way, customized CRISPR plasmids containing specific parts

https://doi.org/10.1021/acssynbio.2c00175
ACS Synth. Biol. 2022, 11, 3629−3643

such as Cas protein, selective marker, gRNA, yeast ORI or bacterial marker can be easily obtained. Once the CRISPR plasmids are assembled, they can be stored in *E. coli* for longer periods. Those plasmids can be also used for template if the parts run out or to avoid PCR-caused mutations; the plasmid modules can be amplified starting from the connectors (overlapping sequence) to produce ready-to-use parts as shown in Figure 2C.

To increase the genome editing efficiency and reproducibility of this method, the importance of the DNA polymerase type to be used for part amplification was underlined. In other words, the plasmid modules had to be completely amplified as their ends are critical for *in vivo* assembly. To this end, an appropriate DNA polymerase synthesizing complete amplicons containing the connectors was used to overcome the shortening problem of the DNA fragments that might be a bottleneck to amplify long amplicons.

ACtivE achieved more than 80% integration for a single gene in the ARS1531 region. For multiplexing, expressing multiple gRNAs through a single plasmid resulted in a higher integration yield for multiloci and multigene integration. More than 50% integration efficiency for triple genes was reached in the ARS1531 region as a single-locus multigene integration. Also, more than 90% deletion efficiency was obtained on the *DIT1* gene. Considering its usefulness and pace, this method should accelerate genome editing processes as the strains of interest can be smoothly detected after a simple screening.

In addition, eight ARS-proximal regions in the yeast genome were thoroughly characterized using two different yeast media. The total biomass and growth rates of the strains containing heterologous genes in the corresponding loci were found. Also, RFUs were detected to characterize the gene expression rates and total protein production in these locations. All strains showed higher growth rates in YPD than in the SD medium. Considering the growth rates, ARS1316 and ARS1531 might be good targets for high biomass in YPD, whereas ARS306 and ARS1603 are preferable for higher biomass in SD media. Nonetheless, no significant difference in the final biomass was observed compared to the parental strain in YPD media. In contrast, strains 209, 727, 1011, and 1316 showed lower growth rates than the parental strain in SD media. On the other hand, gene expression rates might vary depending on the locus used. ARS209 and ARS727 showed better protein expressions in YPD media, while ARS1011 was the best locus for gene expression in SD media. Dynamic gene expression varied considerably mainly depending on the medium conditions, and the cumulative expressions were higher in SD media, although the biomasses were lower in this media.

S. cerevisiae is an important chassis organism for many applications, from metabolic engineering to disease modeling. The CRISPR/Cas system has been a versatile instrument for designing its genome. The improvements and alternative approaches presented in this paper have a great potential to accelerate the yeast genome editing process in a standardizable and easy way. The genomic loci characterized in this study provide more options for well-defined genomic landing sites, especially for yeast cell factory design.

MATERIALS AND METHODS

Oligonucleotides, Reagents, and Plasmids. All primers used in the study are listed in Table S1−S4. The primers were ordered from Integrated DNA Technologies (IDT) as standard DNA oligos for fragments from 20 bp to 100 bp or as DNA ultramers for fragments with ∼120 bp length. Synthetic gRNA cassettes (Figure S1) were ordered from Twist Bioscience. Phusion Flash High-Fidelity PCR Master Mix (Thermo Fisher Scientific) and PrimeSTAR GXL DNA Polymerase (TaKaRa) were used for PCR reactions, while DreamTaq Green PCR Master Mix (Thermo Fisher Scientific) was used for colony PCR. FastDigest DpnI (Thermo Fisher Scientific) was used to degrade the parental plasmids. GeneJET PCR Purification Kit (Thermo Fisher Scientific) was used for PCR cleanup. GeneJET Plasmid Miniprep Kit (Thermo Fisher Scientific) was used for plasmid extraction. p426_Cas9_gRNA-ARS511b (Addgene) was used to amplify uracil auxotrophic selection marker (*URA3*), yeast origin of replication (2 μ ori) and bacteria storage fragment containing ampicillin resistance gene (*AmpR*), and bacterial origin of replication. pWS158 (Addgene) was used as a template to amplify *Cas9* (*Streptococcus pyogenes*) codon-optimized for expression in *Saccharomyces cerevisiae*. mNeonGreen was used as green fluorescence protein (GFP) and it was amplified from pCPS1ULA-BA6 was obtained as a gift from Matthew Dale (Rosser Lab, the University of Edinburgh). pTDH3-Re2.8−2 was gifted by Jamie Auxillos (Chris French Lab, the University of Edinburgh) and red fluorescent protein (RFP), mCherry, was amplified using this plasmid.

Strains and Media. The parent strain of *S. cerevisiae*, BY4741 {MATa; *his3*Δ1; *leu2*Δ0; *met15*Δ0; *ura3*Δ0}, was used for genomic integrations and was kindly provided by Dariusz Abramczyk (Chris French Lab, the University of Edinburgh). *S. cerevisiae* CEN.PK2−1C {MATa; *his3*Δ1; *leu2-3_112*; *ura3-52*; *trp1-289*; *MAL2-8c*; *SUC2*} from EUROSCARF Collection was used for genomic deletions. Unless otherwise stated, all chemicals were sourced from Sigma-Aldrich at the highest available purity. For cultivation of strains, YPD medium containing yeast extract (1% (w/v)), peptone (2% (w/v)), and 2% (w/v) dextrose (glucose) was used. To select positive transformants expressing *URA3* marker, synthetic defined medium containing complete supplement mixture minus uracil (CSM-Ura, MP Biomedicals), 0.17% (w/v) yeast nitrogen base without amino acid, 0.5% (w/v) ammonium sulfate, 2% (w/v) glucose, and 2% (w/v) agar was used. For counter-selection of plasmid-free yeast cells, a synthetic defined medium supplemented with 0.1% (w/v) 5-Fluoroorotic Acid (5-FOA) (Thermo Fisher Scientific) was used. YPD media and complete synthetic defined (SD) media containing all amino acids were used for mNeonGreen expression and characterization of genomic loci.

Yeast Heat-Shock Transformation. The chemicals were sourced from Sigma-Aldrich unless otherwise stated. All transformations were carried out according to LiAc/PEG heat-shock method[69] with some small modifications. After overnight cultures, fresh cultures were prepared to obtain the cells in the exponential phase. The cells were then washed once and were pelleted by centrifugation. The transformation mix containing 240 μL PEG (50% (w/v)), 36 μL 1.0 M lithium acetate (LiAc) and 50 μL single-stranded carrier DNA (2.0 mg/mL) (herring sperm DNA, Promega) were added onto the cell pellet. Next, DNA fragments and water were added until the volume was made up to 360 μL. 50 fmol equivalent molarity of each plasmid-forming DNA part, 500−1000 ng from each donor DNA part were added to the transformation mixes. As a large number of modular fragments were used for multiplexing, transformation volume was increased to 400 μL when needed by adding more DNAs without water addition.

https://doi.org/10.1021/acssynbio.2c00175
ACS Synth. Biol. 2022, 11, 3629−3643

After homogeneous transformation mixes were obtained, the cells were incubated for 45 min at 42 °C. After plating cells to the selective media, the cells were incubated for 2−3 days at 30 °C.

Determination of Genome Editing Efficiency and Plasmid Assembly. When the colonies became visible after integrating *mNeonGreen* into single loci, the plates were imaged on a blue-LED transilluminator (Thermo Fisher Scientific) to distinguish fluorescent mNeonGreen-expressing positive colonies from nonfluorescing negative colonies. Also, colony PCR was performed on randomly selected five positive colonies from each plate to confirm that the genes are integrated into correct locations, and 100% consistency was observed for all positive colonies controlled. Integration efficiency was determined by calculating the percentage of green light-emitting colonies. To count the colonies on the plates when numerous colonies were obtained, ImageJ,[70] a free distribution software, was employed with the Colony Counter plugin (Figure S4).[71] The plate images on the blue-LED transilluminator were first converted to 16-bit pictures. The green colonies (positive) and white colonies (negative) were distinguished using color contrast, and colonies were counted automatically. For integration efficiency of simultaneous integration of *mNeonGreen* and *mCherry*, first, the mNeonGreen expressing colonies were determined on a blue-LED transilluminator. Those colonies were then screened in CLARIOstar Plus microplate reader (BMG Labtech) to detect *mCherry* expression using spectral scanning with an emission wavelength ranging from 580 to 670 nm at 552 nm excitation wavelength. The positive colonies expressing both *mNeonGreen* and *mCherry* were also screened by colony PCR to confirm the integrations. Finally, orange colonies were counted using Colony Counter—ImageJ to determine the integration efficiency of the *β*-carotene pathway. These integrations were also confirmed by employing colony PCR. The genomic deletions were first screened using colony PCR, and the deletions were confirmed by Sanger sequencing performed at GENEWIZ, Inc. (Leipzig, Germany). Correct plasmid assembly was first determined using F1−5 and R1−5 primers (Table S1) flanking the connectors; following that, the whole plasmid was sequenced using primer walking (Seq1−10 in Table S1) by Sanger sequencing.

Characterization of Genomic Loci with *mNeonGreen* Expression. Three individual colonies from each strain expressing *mNeonGreen* on different loci were selected after confirming the integrations. 5-FOA counter-selection was performed to select plasmid-free cells after overnight culture in YPD media. Eight *mNeonGreen* expressing strains and the parent strains, BY4741, were then cultured in YPD and SD media with three replicates for 72 h to observe expression rates of mNeonGreen on each locus. Biomass of different strains was also measured to compare the integration effect on cell fitness. After overnight culture of each strain, cells were inoculated into fresh media to be grown for around six hours to obtain cells in the exponential phase. The initial OD600 was adjusted to 0.1 for the growth experiments for all strains. To avoid sedimentation in low volumes, the cells were grown in 1 mL media, YPD or SD, using 24-well plates (Greiner) with shaking at 200 rpm, at 30 °C. To measure fluorescence intensity and biomass, 20 μL culture samples were taken on the 0th, 3rd, 6th, 12th, 15th, 18th, 21st, 24th, 36th, 48th, and 72nd hours and mixed with water in 200 μL total volume in a black, clear-bottom 96-well plate (Greiner). An anticondensation solution containing 0.05% Triton X-100 (Sigma-Aldrich) in 20% ethanol[72] was used to cover the lids of the well-plates to prevent condensation on the lids. Fluorescence intensities and OD_{600} measurements were taken using the CLARIOstar microplate reader (BMG Labtech). Matrix scan (2 × 2, 25 flashes) was used to scan the wells. To measure mNeonGreen expression, 490 and 525 nm wavelengths were used for excitation and emission, respectively, with 10 nm bandwidth. The emission wavelength was set to 585 nm for autofluorescence of media and yeast cells.[64] The gain was 1500 for both protocols.

Data Analysis and Software. CRISPR experiments were conducted in at least three replicates. The error bars represent the standard deviations of different experiments. The one-way analysis of variance (ANOVA) (p-value <0.05) was used to determine whether there was a statistically significant difference between the experiments. The yeast genome was screened using UCSC Genome Browser[73] (http://genome.ucsc.edu) to find ARS-proximal intergenic regions. The potential 20 bp crRNA sequences on each region were scored using CRISPOR[74] (http://crispor.tefor.net), an online gRNA selection tool giving sequence-based scores using sequence prediction algorithms.[50,51] The linear regression was used to determine the relationship between integration efficiencies and gRNA efficiency prediction scores, and Person's correlation coefficients (R) were calculated employing MATLAB. The fluorescence intensity and OD600 data were analyzed using SciPy package[75] (Matplotlib, NumPy, pandas), *seaborn*,[76] and *omniplate*[65] in Python. Before analyzing growth characteristics, OD correction was performed using a standard curve for 2% (w/v) glucose-containing media as there is a nonlinear relationship between biomass and OD_{600}. To find the actual fluorescence intensity of per mNeonGreen expressing cell, autofluorescence caused by yeast cells themselves and media, YPD or SD, was corrected.[64] To calculate the areas under the curves, the trapezoidal rule was used. The codes and the standard curve used for plate reader data analysis can be found on https://github.com/kmalci/plate-reader. The illustrations were made using BioRender.[77]

■ ASSOCIATED CONTENT

Data Availability Statement

The detailed information about the parts and modules in the toolkit and the version updates can be found at https://www.leorioslab.org/cost-crispr-toolkit/. The codes and the standard curve for plate reader data analysis can be found at https://github.com/kmalci/plate-reader/.

Supporting Information

The Supporting Information is available free of charge at https://pubs.acs.org/doi/10.1021/acssynbio.2c00175.

Primers and DNA fragments used in the study (Table S1−S5); sequence maps (Figure S1−S3); *mNeonGreen* expressing positive colonies (Figure S4); *in vivo* DNA assembly test (Figure S5); characterization of genomic loci in terms of growth rates (Figure S6−S8) and gene expression rates (Figure S9−S11); *β*-carotene producers (Figure S12) (PDF)

■ AUTHOR INFORMATION

Corresponding Author

Leonardo Rios-Solis − *Institute for Bioengineering, School of Engineering, University of Edinburgh, Edinburgh EH9 3BF,*

https://doi.org/10.1021/acssynbio.2c00175
ACS Synth. Biol. 2022, 11, 3629−3643

U.K.; Centre for Synthetic and Systems Biology (SynthSys), University of Edinburgh, Edinburgh EH9 3BD, U.K.; School of Natural and Environmental Sciences, Newcastle University, Newcastle upon Tyne NE1 7RU, U.K.; orcid.org/0000-0002-4387-984X; Email: leo.rios@newcastle.ac.uk

Authors

Koray Malcı − *Institute for Bioengineering, School of Engineering, University of Edinburgh, Edinburgh EH9 3BF, U.K.; Centre for Synthetic and Systems Biology (SynthSys), University of Edinburgh, Edinburgh EH9 3BD, U.K.;* orcid.org/0000-0002-2942-1146

Nestor Jonguitud-Borrego − *Institute for Bioengineering, School of Engineering, University of Edinburgh, Edinburgh EH9 3BF, U.K.; Centre for Synthetic and Systems Biology (SynthSys), University of Edinburgh, Edinburgh EH9 3BD, U.K.*

Hugo van der Straten Waillet − *Institute for Bioengineering, School of Engineering, University of Edinburgh, Edinburgh EH9 3BF, U.K.*

Urtė Puodžiūnaitė − *Institute for Bioengineering, School of Engineering, University of Edinburgh, Edinburgh EH9 3BF, U.K.; Centre for Synthetic and Systems Biology (SynthSys), University of Edinburgh, Edinburgh EH9 3BD, U.K.; School of Biological Sciences, University of Edinburgh, Edinburgh EH9 3FF, U.K.*

Emily J. Johnston − *Centre for Synthetic and Systems Biology (SynthSys), University of Edinburgh, Edinburgh EH9 3BD, U.K.; School of Biological Sciences, University of Edinburgh, Edinburgh EH9 3FF, U.K.*

Susan J. Rosser − *Centre for Synthetic and Systems Biology (SynthSys), University of Edinburgh, Edinburgh EH9 3BD, U.K.; School of Biological Sciences, University of Edinburgh, Edinburgh EH9 3FF, U.K.*

Complete contact information is available at: https://pubs.acs.org/10.1021/acssynbio.2c00175

Author Contributions

KM and LR-S conceived the study. KM designed the experiments and performed the data analysis. KM, NJ-B, HvdSW, UP, and EJJ performed the experiments. KM drafted the manuscript. EJJ, SJR, and LR-S assisted with writing, editing, and finalizing the manuscript. All of the authors have read and approved the final version of the manuscript.

Notes

The authors declare no competing financial interest.

■ ACKNOWLEDGMENTS

This study was supported by the YLSY Program of the Ministry of National Education of the Republic of Turkey, the British Council (Grant Number: 527429894), IBCatalyst (Project No. 102297), and Biotechnology and Biological Sciences Research Council (BBSRC; Project BB/S017712/1). The authors thank Dr. Dariusz Abramczyk for providing the BY4741 strain, Dr. Matthew Dale for his gift of vector pCPS1ULA-BA6, Dr. Jamie Auxillos for her gift of pTDH3-Re2.8-2 vector, Alexander Speakman for technical assistance about the microplate reader, and Prof. Peter Swain for his guidance on the *omniplate* software.

■ REFERENCES

(1) Walls, L. E.; Malcı, K.; Nowrouzi, B.; Li, R. A.; D'Espaux, L.; Wong, J.; Dennis, J. A.; Semião, A. J. C.; Wallace, S.; Martinez, J. L.; Keasling, J. D.; Rios-Solis, L. Optimizing the Biosynthesis of Oxygenated and Acetylated Taxol Precursors in Saccharomyces Cerevisiae Using Advanced Bioprocessing Strategies. *Biotechnol. Bioeng.* **2021**, *118* (1), 279−293.

(2) Nowrouzi, B.; Li, R.; Walls, L. E.; D'Espaux, L.; Malci, K.; Liang, L.; Jonguitud Borrego, N.; Lerma Escalera, A. I.; Morones-Ramirez, J. R.; Keasling, J. D.; Rios Solis, L. Enhanced Production of Taxadiene in Saccharomyces Cerevisiae. *Microb. Cell Factories* **2020**, *19*, 200.

(3) Madhavan, A.; Arun, K. B.; Sindhu, R.; Krishnamoorthy, J.; Reshmy, R.; Sirohi, R.; Pugazhendi, A.; Awasthi, M. K.; Szakacs, G.; Binod, P. Customized Yeast Cell Factories for Biopharmaceuticals: From Cell Engineering to Process Scale Up. *Microb. Cell Fact.* **2021**, *20* (1), 1−17.

(4) Wong, J.; de Rond, T.; d'Espaux, L.; van der Horst, C.; Dev, I.; Rios-Solis, L.; Kirby, J.; Scheller, H.; Keasling, J. High-Titer Production of Lathyrane Diterpenoids from Sugar by Engineered Saccharomyces Cerevisiae. *Metab. Eng.* **2018**, *45*, 142−148.

(5) Nielsen, J.; Larsson, C.; van Maris, A.; Pronk, J. Metabolic Engineering of Yeast for Production of Fuels and Chemicals. *Curr. Opin. Biotechnol.* **2013**, *24* (3), 398−404.

(6) Mohd Azhar, S. H.; Abdulla, R.; Jambo, S. A.; Marbawi, H.; Gansau, J. A.; Mohd Faik, A. A.; Rodrigues, K. F. Yeasts in Sustainable Bioethanol Production: A Review. *Biochem. Biophys. Reports* **2017**, *10*, 52−61.

(7) Walls, L. E.; Rios-Solis, L. Sustainable Production of Microbial Isoprenoid Derived Advanced Biojet Fuels Using Different Generation Feedstocks: A Review. *Front. Bioeng. Biotechnol.* **2020**, *8*, 1272.

(8) Wong, J.; Rios-Solis, L.; Keasling, J. D. Microbial Production of Isoprenoids. *Consequences Microb. Interact. with Hydrocarb. Oils, Lipids Prod. Fuels Chem.* **2017**, 359−382.

(9) Ding, W.; Zhang, Y.; Shi, S. Development and Application of CRISPR/Cas in Microbial Biotechnology. *Front. Bioeng. Biotechnol.* **2020**, *8*, 711.

(10) Meng, J.; Qiu, Y.; Shi, S. CRISPR/Cas9 Systems for the Development of Saccharomyces Cerevisiae Cell Factories. *Front. Bioeng. Biotechnol.* **2020**, *8*, 594347.

(11) Stovicek, V.; Holkenbrink, C.; Borodina, I. CRISPR/Cas System for Yeast Genome Engineering: Advances and Applications. *FEMS Yeast Res.* **2017**, *17* (5), 30.

(12) Malcı, K.; Walls, L. E.; Rios-Solis, L. Multiplex Genome Engineering Methods for Yeast Cell Factory Development. *Front. Bioeng. Biotechnol.* **2020**, *8*, 1264.

(13) Hille, F.; Charpentier, E. CRISPR-Cas: Biology, Mechanisms and Relevance. *Philos. Trans. R. Soc. B Biol. Sci.* **2016**, DOI: 10.1098/RSTB.2015.0496.

(14) Richter, C.; Chang, J. T.; Fineran, P. C. Function and Regulation of Clustered Regularly Interspaced Short Palindromic Repeats (CRISPR)/CRISPR Associated (Cas) Systems. *Viruses* **2012**, *4* (10), 2291.

(15) Deaner, M.; Alper, H. S. Systematic Testing of Enzyme Perturbation Sensitivities via Graded DCas9Modulation in Saccharomyces Cerevisiae. *Metab. Eng.* **2017**, *40*, 14−22.

(16) Generoso, W. C.; Gottardi, M.; Oreb, M.; Boles, E. Simplified CRISPR-Cas Genome Editing for Saccharomyces Cerevisiae. *J. Microbiol. Methods* **2016**, *127*, 203−205.

(17) Zalatan, J. G.; Lee, M. E.; Almeida, R.; Gilbert, L. A.; Whitehead, E. H.; La Russa, M.; Tsai, J. C.; Weissman, J. S.; Dueber, J. E.; Qi, L. S.; Lim, W. A. Engineering Complex Synthetic Transcriptional Programs with CRISPR RNA Scaffolds. *Cell* **2015**, *160*, 339.

(18) Vanegas, K. G.; Lehka, B. J.; Mortensen, U. H. SWITCH: A Dynamic CRISPR Tool for Genome Engineering and Metabolic Pathway Control for Cell Factory Construction in Saccharomyces Cerevisiae. *Microb. Cell Fact.* **2017**, *16* (1), 25.

(19) Laughery, M. F.; Hunter, T.; Brown, A.; Hoopes, J.; Ostbye, T.; Shumaker, T.; Wyrick, J. J. New Vectors for Simple and Streamlined CRISPR-Cas9 Genome Editing in Saccharomyces Cerevisiae. *Yeast* **2015**, *32* (12), 711.

(20) Jakočiunas, T.; Bonde, I.; Herrgård, M.; Harrison, S. J.; Kristensen, M.; Pedersen, L. E.; Jensen, M. K.; Keasling, J. D. Multiplex Metabolic Pathway Engineering Using CRISPR/Cas9 in Saccharomyces Cerevisiae. *Metab. Eng.* **2015**, *28*, 213−222.
(21) Zhang, G.-C.; Kong, I. I.; Kim, H.; Liu, J.-J.; Cate, J. H. D.; Jin, Y.-S. Construction of a Quadruple Auxotrophic Mutant of an Industrial Polyploid Saccharomyces Cerevisiae Strain by Using RNA-Guided Cas9 Nuclease. *Appl. Environ. Microbiol.* **2014**, *80* (24), 7694.
(22) Symington, L. S.; Gautier, J. Double-Strand Break End Resection and Repair Pathway Choice. *Annu. Rev. Genet.* **2011**, *45*, 247−271.
(23) DiCarlo, J. E.; Norville, J. E.; Mali, P.; Rios, X.; Aach, J.; Church, G. M. Genome Engineering in Saccharomyces Cerevisiae Using CRISPR-Cas Systems. *Nucleic Acids Res.* **2013**, *41* (7), 4336.
(24) Ryan, O. W.; Skerker, J. M.; Maurer, M. J.; Li, X.; Tsai, J. C.; Poddar, S.; Lee, M. E.; DeLoache, W.; Dueber, J. E.; Arkin, A. P.; Cate, J. H. Selection of Chromosomal DNA Libraries Using a Multiplex CRISPR System. *eLife* **2014**, *3*, 1−15.
(25) Ronda, C.; Maury, J.; Jakočiŭnas, T.; Baallal Jacobsen, S. A.; Germann, S. M.; Harrison, S. J.; Borodina, I.; Keasling, J. D.; Jensen, M. K.; Nielsen, A. T. CrEdit: CRISPR Mediated Multi-Loci Gene Integration in Saccharomyces Cerevisiae. *Microb. Cell Fact.* **2015**, *14* (1), 97.
(26) Malcı, K.; Watts, E.; Roberts, T. M.; Auxillos, J. Y.; Nowrouzi, B.; Boll, H. O.; Nascimento, C. Z. S. do; Andreou, A.; Vegh, P.; Donovan, S.; Fragkoudis, R.; Panke, S.; Wallace, E.; Elfick, A.; Rios-Solis, L. Standardization of Synthetic Biology Tools and Assembly Methods for Saccharomyces Cerevisiae and Emerging Yeast Species. *ACS Synth. Biol.* **2022**, *11* (8), 2527−2547.
(27) Engler, C.; Kandzia, R.; Marillonnet, S. A One Pot, One Step, Precision Cloning Method with High Throughput Capability. *PLoS One* **2008**, *3* (11), No. e3647.
(28) Gibson, D. G.; Young, L.; Chuang, R.-Y.; Venter, J. C.; Hutchison, C. A.; Smith, H. O. Enzymatic Assembly of DNA Molecules up to Several Hundred Kilobases. *Nat. Methods* **2009**, *6* (5), 343−345.
(29) Nour-Eldin, H. H.; Hansen, B. G.; Nørholm, M. H. H.; Jensen, J. K.; Halkier, B. A. Advancing Uracil-Excision Based Cloning towards an Ideal Technique for Cloning PCR Fragments. *Nucleic Acids Res.* **2006**, *34* (18), No. e122.
(30) Akhmetov, A.; Laurent, J. M.; Gollihar, J.; Gardner, E. C.; Garge, R. K.; Ellington, A. D.; Kachroo, A. H.; Marcotte, E. M. Single-Step Precision Genome Editing in Yeast Using CRISPR-Cas9. *Bio-protocol* **2018**, DOI: 10.21769/BioProtoc.2765.
(31) Bao, Z.; Xiao, H.; Liang, J.; Zhang, L.; Xiong, X.; Sun, N.; Si, T.; Zhao, H. Homology-Integrated CRISPR-Cas (HI-CRISPR) System for One-Step Multigene Disruption in Saccharomyces Cerevisiae. *ACS Synth. Biol.* **2015**, *4* (5), 585−594.
(32) Jakočiunas, T.; Bonde, I.; Herrgård, M.; Harrison, S. J.; Kristensen, M.; Pedersen, L. E.; Jensen, M. K.; Keasling, J. D. Multiplex Metabolic Pathway Engineering Using CRISPR/Cas9 in Saccharomyces Cerevisiae. *Metab. Eng.* **2015**, *28*, 213−222.
(33) Ferreira, R.; Skrekas, C.; Nielsen, J.; David, F. Multiplexed CRISPR/Cas9 Genome Editing and Gene Regulation Using Csy4 in Saccharomyces Cerevisiae. *ACS Synth. Biol.* **2018**, *7* (1), 10−15.
(34) NEB Golden Gate Assembly Kit (BsaI-HFv2) | NEB. https://international.neb.com/products/e1601-neb-golden-gate-assembly-mix#Product%20Information (accessed on August 26, 2021).
(35) Gibson Assembly Cloning Kit | NEB. https://international.neb.com/products/e5510-gibson-assembly-cloning-kit#Product%20Information (accessed on August 26, 2021).
(36) Shevchuk, N. A.; Bryksin, A. V.; Nusinovich, Y. A.; Cabello, F. C.; Sutherland, M.; Ladisch, S. Construction of Long DNA Molecules Using Long PCR-Based Fusion of Several Fragments Simultaneously. *Nucleic Acids Res.* **2004**, *32* (2), No. e19.
(37) Karvelis, T.; Gasiunas, G.; Miksys, A.; Barrangou, R.; Horvath, P.; Siksnys, V. CrRNA and TracrRNA Guide Cas9-Mediated DNA Interference in Streptococcus Thermophilus. *RNA Biol.* **2013**, *10* (5), 841.
(38) Wilson, L. O. W.; O'Brien, A. R.; Bauer, D. C. The Current State and Future of CRISPR-Cas9 GRNA Design Tools. *Front. Pharmacol.* **2018**, DOI: 10.3389/fphar.2018.00749.
(39) Zhang, T.; Gao, Y.; Wang, R.; Zhao, Y. Production of Guide RNAs in Vitro and in Vivo for CRISPR Using Ribozymes and RNA Polymerase II Promoters. *Bio-protocol* **2017**, DOI: 10.21769/BioProtoc.2148.
(40) Horlbeck, M. A.; Witkowsky, L. B.; Guglielmi, B.; Replogle, J. M.; Gilbert, L. A.; Villalta, J. E.; Torigoe, S. E.; Tjian, R.; Weissman, J. S. Nucleosomes Impede Cas9 Access to DNA in Vivo and in Vitro. *eLife* **2016**, DOI: 10.7554/eLife.12677.
(41) Reider Apel, A.; d'Espaux, L.; Wehrs, M.; Sachs, D.; Li, R. A.; Tong, G. J.; Garber, M.; Nnadi, O.; Zhuang, W.; Hillson, N. J.; Keasling, J. D.; Mukhopadhyay, A. A Cas9-Based Toolkit to Program Gene Expression in *Saccharomyces Cerevisiae*. *Nucleic Acids Res.* **2017**, *45* (1), 496−508.
(42) Wu, X.-L.; Li, B.-Z.; Zhang, W.-Z.; Song, K.; Qi, H.; Dai, J.; Yuan, Y.-J. Genome-Wide Landscape of Position Effects on Heterogeneous Gene Expression in Saccharomyces Cerevisiae. *Biotechnol. Biofuels* **2017**, *10* (1), 1−10.
(43) Gibson, D. G.; Benders, G. A.; Axelrod, K. C.; Zaveri, J.; Algire, M. A.; Moodie, M.; Montague, M. G.; Venter, J. C.; Smith, H. O.; Hutchison, C. A. One-Step Assembly in Yeast of 25 Overlapping DNA Fragments to Form a Complete Synthetic Mycoplasma Genitalium Genome. *Proc. Natl. Acad. Sci. U. S. A.* **2008**, *105* (51), 20404−20409.
(44) Kuijpers, N. G.; Solis-Escalante, D.; Bosman, L.; van den Broek, M.; Pronk, J. T.; Daran, J.-M.; Daran-Lapujade, P. A Versatile, Efficient Strategy for Assembly of Multi-Fragment Expression Vectors in Saccharomyces Cerevisiae Using 60 Bp Synthetic Recombination Sequences. *Microb. Cell Fact.* **2013**, *12* (1), 1−13.
(45) Eisenstein, M. Enzymatic DNA Synthesis Enters New Phase. *Nat. Biotechnol.* **2020**, *38* (10), 1113−1115.
(46) Hughes, R. A.; Ellington, A. D. Synthetic DNA Synthesis and Assembly: Putting the Synthetic in Synthetic Biology. *Cold Spring Harb. Perspect. Biol.* **2017**, *9* (1), a023812.
(47) Portela, R. M. C.; Vogl, T.; Kniely, C.; Fischer, J. E.; Oliveira, R.; Glieder, A. Synthetic Core Promoters as Universal Parts for Fine-Tuning Expression in Different Yeast Species. *ACS Synth. Biol.* **2017**, *6* (3), 471−484.
(48) Flagfeldt, D. B.; Siewers, V.; Huang, L.; Nielsen, J. Characterization of Chromosomal Integration Sites for Heterologous Gene Expression in Saccharomyces Cerevisiae. *Yeast* **2009**, *26* (10), 545−551.
(49) Wu, X. Le.; Bi, Y. H.; Gao, F.; Xie, Z. X.; Li, X.; Zhou, X.; Ma, D. J.; Li, B. Z.; Yuan, Y. J. The Effect of Autonomously Replicating Sequences on Gene Expression in Saccharomyces Cerevisiae. *Biochem. Eng. J.* **2019**, *149*, 107250.
(50) Moreno-Mateos, M. A.; Vejnar, C. E.; Beaudoin, J.-D.; Fernandez, J. P.; Mis, E. K.; Khokha, M. K.; Giraldez, A. J. CRISPRscan: Designing Highly Efficient SgRNAs for CRISPR-Cas9 Targeting in Vivo. *Nat. Methods* **2015**, *12* (10), 982−988.
(51) Doench, J. G.; Fusi, N.; Sullender, M.; Hegde, M.; Vaimberg, E. W.; Donovan, K. F.; Smith, I.; Tothova, Z.; Wilen, C.; Orchard, R.; Virgin, H. W.; Listgarten, J.; Root, D. E. Optimized SgRNA Design to Maximize Activity and Minimize Off-Target Effects of CRISPR-Cas9. *Nat. Biotechnol.* **2016**, *34* (2), 184−191.
(52) Hsu, P. D.; Scott, D. A.; Weinstein, J. A.; Ran, F. A.; Konermann, S.; Agarwala, V.; Li, Y.; Fine, E. J.; Wu, X.; Shalem, O.; Cradick, T. J.; Marraffini, L. A.; Bao, G.; Zhang, F. DNA Targeting Specificity of RNA-Guided Cas9 Nucleases. *Nat. Biotechnol.* **2013**, *31* (9), 827−832.
(53) Stratigopoulos, G.; De Rosa, M. C.; LeDuc, C. A.; Leibel, R. L.; Doege, C. A. DMSO Increases Efficiency of Genome Editing at Two Non-Coding Loci. *PLoS One* **2018**, *13* (6), No. e0198637.
(54) Beal, J.; Goñi-Moreno, A.; Myers, C.; Hecht, A.; del Carmen Vicente, M.; Parco, M.; Schmidt, M.; Timmis, K.; Baldwin, G.;

Friedrichs, S.; Freemont, P.; Kiga, D.; Ordozgoiti, E.; Rennig, M.; Rios, L.; Tanner, K.; Lorenzo, V.; Porcar, M. The Long Journey towards Standards for Engineering Biosystems. *EMBO Rep.* **2020**, DOI: 10.15252/embr.202050521.
(55) Why PCR product can't be re-amplified in second round?https://www.researchgate.net/post/Why_PCR_product_cant_be_re-amplified_in_second_round (accessed on September 1, 2021).
(56) Gao, S.; Honey, S.; Futcher, B.; Grollman, A. P. The Non-Homologous End-Joining Pathway of S. Cerevisiae Works Effectively in G1-Phase Cells, and Religates Cognate Ends Correctly and Non-Randomly. *DNA Repair (Amst).* **2016**, *42*, 1.
(57) Emerson, C. H.; Bertuch, A. A. Consider the Workhorse: Nonhomologous End Joining in Budding Yeast. *Biochem. Cell Biol.* **2016**, *94* (5), 396.
(58) Jang, I.-S.; Yu, B. J.; Jang, J. Y.; Jegal, J.; Lee, J. Y. Improving the Efficiency of Homologous Recombination by Chemical and Biological Approaches in Yarrowia Lipolytica. *PLoS One* **2018**, *13* (3), e0194954.
(59) Dong, C.; Jiang, L.; Xu, S.; Huang, L.; Cai, J.; Lian, J.; Xu, Z. A Single Cas9-VPR Nuclease for Simultaneous Gene Activation, Repression, and Editing in Saccharomyces Cerevisiae. *ACS Synth. Biol.* **2020**, *9* (9), 2252−2257.
(60) Buitrago, D.; Labrador, M.; Arcon, J. P.; Lema, R.; Flores, O.; Esteve-Codina, A.; Blanc, J.; Villegas, N.; Bellido, D.; Gut, M.; Dans, P. D.; Heath, S. C.; Gut, I. G.; Brun Heath, I.; Orozco, M. Impact of DNA Methylation on 3D Genome Structure. *Nat. Commun.* **2021**, *12* (1), 1−17.
(61) Hahn-Hägerdal, B.; Karhumaa, K.; Larsson, C. U.; Gorwa-Grauslund, M.; Görgens, J.; van Zyl, W. H. Role of Cultivation Media in the Development of Yeast Strains for Large Scale Industrial Use. *Microb. Cell Fact.* **2005**, *4* (1), 1−16.
(62) Dymond, J. S. Saccharomyces Cerevisiae Growth Media. *Methods Enzymol.* **2013**, *533*, 191−204.
(63) Swain, P. S.; Stevenson, K.; Leary, A.; Montano-Gutierrez, L. F.; Clark, I. B. N.; Vogel, J.; Pilizota, T. Inferring Time Derivatives Including Cell Growth Rates Using Gaussian Processes. *Nat. Commun.* **2016**, *7* (1), 1−8.
(64) Lichten, C. A.; White, R.; Clark, I. B.; Swain, P. S. Unmixing of Fluorescence Spectra to Resolve Quantitative Time-Series Measurements of Gene Expression in Plate Readers. *BMC Biotechnol.* **2014**, *14* (1), 1−11.
(65) *omniplate*. https://swainlab.bio.ed.ac.uk/software/platereader/omniplate.html (accessed on August 29, 2021).
(66) Ringel, A. E.; Ryznar, R.; Picariello, H.; Huang, K. l.; Lazarus, A. G.; Holmes, S. G. Yeast Tdh3 (Glyceraldehyde 3-Phosphate Dehydrogenase) Is a Sir2-Interacting Factor That Regulates Transcriptional Silencing and RDNA Recombination. *PLoS Genet.* **2013**, *9* (10), e1003871.
(67) Pilauri, V.; Bewley, M.; Diep, C.; Hopper, J. Gal80 Dimerization and the Yeast GAL Gene Switch. *Genetics* **2005**, *169* (4), 1903.
(68) Briza, P.; Eckerstorfer, M.; Breitenbach, M. The Sporulation-Specific Enzymes Encoded by the DIT1 and DIT2 Genes Catalyze a Two-Step Reaction Leading to a Soluble LL-Dityrosine-Containing Precursor of the Yeast Spore Wall. *Proc. Natl. Acad. Sci. U. S. A.* **1994**, *91* (10), 4524−4528.
(69) SnapGene | Software for everyday molecular biology.https://www.snapgene.com/ (accessed on August 28, 2021).
(70) Schneider, C. A.; Rasband, W. S.; Eliceiri, K. W. NIH Image to ImageJ: 25 Years of Image Analysis. *Nat. Methods* **2012**, *9* (7), 671−675.
(71) Colony Counter. https://imagej.nih.gov/ij/plugins/colony-counter.html (accessed on August 29, 2021).
(72) Brewster, J. D. A Simple Micro-Growth Assay for Enumerating Bacteria. *J. Microbiol. Methods* **2003**, *53* (1), 77−86.
(73) Karolchik, D.; Baertsch, R.; Diekhans, M.; Furey, T. S.; Hinrichs, A.; Lu, Y. T.; Roskin, K. M.; Schwartz, M.; Sugnet, C. W.; Thomas, D. J.; Weber, R. J.; Haussler, D.; Kent, W. J. The UCSC Genome Browser Database. *Nucleic Acids Res.* **2003**, *31* (1), 51.
(74) Concordet, J.-P.; Haeussler, M. CRISPOR: Intuitive Guide Selection for CRISPR/Cas9 Genome Editing Experiments and Screens. *Nucleic Acids Res.* **2018**, *46* (W1), W242−W245.
(75) Virtanen, P.; Gommers, R.; Oliphant, T. E.; Haberland, M.; Reddy, T.; Cournapeau, D.; Burovski, E.; Peterson, P.; Weckesser, W.; Bright, J.; van der Walt, S. J.; Brett, M.; Wilson, J.; Millman, K. J.; Mayorov, N.; Nelson, A. R. J.; Jones, E.; Kern, R.; Larson, E.; Carey, C. J.; Polat, İ.; Feng, Y.; Moore, E. W.; VanderPlas, J.; Laxalde, D.; Perktold, J.; Cimrman, R.; Henriksen, I.; Quintero, E. A.; Harris, C. R.; Archibald, A. M.; Ribeiro, A. H.; Pedregosa, F.; van Mulbregt, P.; et al. SciPy 1.0: Fundamental Algorithms for Scientific Computing in Python. *Nat. Methods* **2020**, *17* (3), 261−272.
(76) Waskom, M. L. Seaborn: Statistical Data Visualization. *J. Open Source Softw.* **2021**, *6* (60), 3021.
(77) BioRender. https://biorender.com/ (accessed on October 23, 2021).

https://doi.org/10.1021/acssynbio.2c00175
ACS Synth. Biol. 2022, 11, 3629−3643